


## Rotation Curve Fitting Model

SOPHIA NATALIA CISNEROS <sup>1</sup> RICHARD OTT,<sup>2,3</sup> MEAGAN CROWLEY,<sup>4,5</sup> AMY ROBERTS,<sup>6</sup> MARCUS PAZ,<sup>7</sup>  
ZANEEYIAH BROWN,<sup>7</sup> LONDON JOYAL,<sup>7</sup> ROBERTO REAL RICO,<sup>7</sup> ELIZABETH GUTIERREZ-GUTIERREZ,<sup>7</sup> PHONG PHAM,<sup>7</sup>  
ZAC HOLLAND,<sup>7</sup> AMANDA LIVINGSTON,<sup>7,8</sup> LILY CASTRELLON,<sup>7</sup> SUMMER GRAHAM,<sup>7</sup> SHANON J. RUBIN,<sup>9,10</sup>  
AARON ASHLEY,<sup>2,11</sup> DILLON BATTAGLIA,<sup>2</sup> DANIEL LOPEZ,<sup>1</sup> AND MAYA SALWA<sup>1</sup>

<sup>1</sup>*Department of Astronomy  
University of Washington*

<sup>2</sup>*Massachusetts Institute of Technology*

<sup>3</sup>*The Data Incubator*

<sup>4</sup>*University of Massachusetts Boston*

<sup>5</sup>*Colorado School of Mines*

<sup>6</sup>*University of Colorado Denver*

<sup>7</sup>*University of Denver*

<sup>8</sup>*University of New Mexico*

<sup>9</sup>*Boston University*

<sup>10</sup>*University of California Davis*

<sup>11</sup>*Raytheon*

### ABSTRACT

One key piece of evidence for dark matter is the flat rotation curve problem: the disagreement between measured galactic rotation curves and their luminous mass. A novel solution to this problem is presented here. A model of relativistic frame effects on Doppler shifts due to the slightly curved frames of an emitting galaxy with respect to the Milky Way frame is derived. This model predicts observed Doppler shifted spectra based only on the observed luminous matter profile and one free model parameter. The rotation curve fitting model presented is tested on the SPARC sample of 175 galactic rotation profiles using accurate photometry measurements which has previously been fitted by dark matter models, MOND and the Radial Acceleration Relation. For the SPARC sample of 175 galaxies, the new model fits 172 galaxies with an averaged reduced  $\chi_r^2 = 2.25$ , the isothermal dark matter model fits 165 galaxies with an average  $\chi_r^2 = 1.90$ , and the Radial Acceleration Relation fits all 175 galaxies with an average  $\chi_r^2 = 4.22$ . The model presented here has fewer free parameters than either dark matter models or MOND, and does not modify classical physics. Implications of this model are discussed.

*Keywords:* Dark matter (353) — Milky Way dark matter halo (1049) — Galaxy dark matter halos (1880) — Galaxy rotation curves (619)

### 1. INTRODUCTION

The flat-rotation curve problem is the divergence of two rotation velocities about the center of a spiral galaxy, inferred from different observations of light (Rubin et al. 1980; Bosma 1981; van Albada et al. 1985): photometry and Doppler shifted spectra. Photometry gives estimates of the luminous mass, which when interpreted classically by the Poisson equation gives the expected, Keplerian orbital velocities which decline beyond the stars. Doppler shifted spectra, however, gives the “flat-rotation curve” velocities, which remain essentially constant far past the stars. The divergence of these two velocities is primary evidence for dark matter theories (Fig. 3).

Dark matter is hypothesized to be massive particles which are electromagnetically neutral, and have a very low interaction probability with baryonic matter, but otherwise obey classical gravity. Though direct detection experiments continue, in the absence of a definitive observation of such particles (Cebrián 2022), the phenomenological details of dark matter problems remain interesting. S. McGaugh notes a degeneracy between the luminous and dark matter components in a galaxy, when he asks “Why is the luminous tail wagging the dark matter dog, if dark matter dominates dynamics?” (McGaugh 1999). This references the curious fact that knowledge of the stellar disk completely determines the spherical dark matter halo, even though dark matter is postulated to dominate dynamics (McGaugh 2004).

Another interesting trend is the Universal Rotation Curve (URC), in which a spectrum of 1,100 rotation curves (RCs) inflect about the presumed rotation curve of the Milky Way (Persic et al. 1996; Rubin et al. 1978; Salucci et al. 2007). In the URC spectrum, galaxy RCs are separated with respect to the luminous mass of the Milky Way, where the RCs of galaxies larger than the Milky Way inflect downwards “flat”, and RCs of galaxies smaller than the Milky Way inflect upwards towards “flat”. The Milky Way has been postulated to be at the inflection point where truly flat RCs lie, though a definitive rotation curve past our position at approximately 8 kpc has been difficult to constrain until the current era of observations from Gaia DR3 (Jiao, Yongjun et al. 2023). We interpret this positioning of the Milky Way as evidence for frame dependent effects in this problem.

Dark matter theory accounts for the curious URC phenomenology with the phrasing that galaxies smaller than the Milky Way are “dark matter dominated”, and those larger than the Milky Way require only “minimal dark matter halos”. Dark matter particles are designed to obey classical gravity, and so this logical inconsistency means that dark matter models require fine-tuning to account for the URC phenomenology, reducing the predictivity of the models (McGaugh 2021). In classical gravity, mass accretion rates are directly proportional to the initial mass function (Maschberger et al. 2014). Interpreting the URC, instead, from the paradigm of relative frame effects removes this conflict, explains why galaxy RCs are binned as they are with respect to the Milky Way in the URC, removes extraneous free parameters and does not modify classical gravity theory.

The leading alternative to dark matter, Modified Newtonian Dynamics (MOND) (Milgrom 1983), successfully fits a diverse distribution of galaxy RC, by modifying the standard gravitational acceleration scale  $G$  on the length scales of galaxies (McGaugh 2014). In MOND the luminous mass is the only mass, but excesses in Doppler shifted spectra are still interpreted as physical rotation velocities, as in dark matter theories. It is remarkable in that MOND’s free parameter is essentially constant across a wide range of galaxy morphologies (Lelli et al. 2016), though there are some notable exceptions where MOND fits of well-studied galaxies indicate distances which are in conflict with standard candles. Previous attempts to extend MOND to the relativistic regime have given rise to new theories of gravity (Bekenstein 2004; Cooperstock & Tieu 2007; Famaey & McGaugh 2012).

The new rotation curve fitting formula presented here fits the same galaxies as MOND and dark matter, at reported distances, with fewer free parameters. The only inputs to the RCFM fits are estimates of the luminous mass of the galaxy being observed and that of the Milky Way. Luminous mass models used here are those reported in the SPARC database (Lelli et al. 2016), with the addition of a few other galaxies for the sake of comparison in figures. Recent observations of the Milky Way from the Gaia DR3, indicate a Keplerian decline in rotation velocities to 26 kpc, consistent with the model paradigm presented here Jiao, Yongjun et al. (2023).

The new rotation curve fitting model (RCFM) is derived in **Section 2**. Previous consideration of relative gravitational frame effects in the flat-rotation curve problem used Galilean differences of redshifts at the large  $r$  limit of the observations (Misner et al. 1973), instead of the Lorentz-type maps used here. In **Section 3** we describe the SPARC database of 175 well known galaxy rotation curves and associated luminous mass models, and the Milky Way baryon models used in this work. In **Section 4** we compare RCFM fit results to those from dark matter and the Radial Acceleration Relation (RAR) models for the SPARC galaxies. The RAR is an empirical relation (McGaugh 2014; McGaugh et al. 2016; Lelli et al. 2016; Li et al. 2018), postulated to be the phenomenological basis of MOND (Dutton et al. 2019). In this section we also explore a correlation between the RCFM free parameter and a ratio of photometric observables (luminosity and half light radius of the galaxy). In **Section 5** we conclude with discussion of upcoming observations which can further constrain or falsify this model.

## 2. ROTATION CURVE FITTING MODELS

### 2.1. Two observations of light

The observables in the flat-rotation curve problem are the Doppler shifted spectra and photometry. Doppler shifted spectra give RC velocities  $v_{obs}(r)$  by Lorentz boost

$$\frac{v_{obs}(r)}{c} = \frac{\left(\frac{\omega'(r)}{\omega_o}\right) - \left(\frac{\omega_o}{\omega'(r)}\right)}{\left(\frac{\omega'(r)}{\omega_o}\right) + \left(\frac{\omega_o}{\omega'(r)}\right)}, \quad (1)$$

for  $\omega_o$  the characteristic lab frequency and  $\omega'(r)$  the observed shifted frequency.  $c$  is the vacuum light speed. We emphasize this form of the Lorentz boost is applicable to a flat, inertial spacetime.

The second observable, photometry, gives a measure of total light which is then interpreted as mass from population synthesis models (PSMs) which produce mass-to-light ratios and hence models of the baryon distribution in a given galaxy. PSM rely upon a complex suite of assumptions regarding galaxy evolution, metallicities and initial mass functions (Bell & de Jong 2001; Schombert et al. 2018), and are under-constrained due to the dark matter problem (Conroy et al. 2009; Dutton et al. 2005), producing an error budget of  $\approx 20\%$  (Lelli et al. 2016).

Mass models give velocities by parametrizing the integration of the Newtonian gravitational potential by

$$\Phi(r) = - \int_{r_{ref}}^r \vec{g} \cdot d\vec{r}. \quad (2)$$

for  $r$  the field point,  $r_{ref}$  the reference point, and  $g$  the acceleration due to the gravitational field. The classical boundary condition is that the potential goes to zero at  $r' = \infty$ , hence the integration effectively starts from large  $r_{ref} = R$  into the small  $r$  limit of the data. This potential then solves the Poisson equation

$$\nabla^2 \Phi(r)_{lum} = 4\pi G \rho(r'), \quad (3)$$

where  $\rho(r')$  is the mass density distribution and  $G$  is Newton's constant. The gradient of this potential then gives the circular orbital velocities  $v(r)_{lum}$  (Eq. 6) by the central force relation

$$\frac{\partial \Phi(r)_{lum}}{\partial r} = \frac{v(r)_{lum}^2}{r}. \quad (4)$$

The baryonic components are summed in quadrature as stellar disk, stellar bulge, and a gas halo

$$v(r)_{lum}^2 = \gamma_b v(r)_{bulge}^2 + \gamma_d v(r)_{disk}^2 + v(r)_{gas}^2. \quad (5)$$

where  $\gamma_b$  and  $\gamma_d$  are the stellar mass-to-light ratios, which are free parameters in rotation curve fits. Gas fractions  $v(r)_{gas}$  are calculated from a different observational technique as given in Casertano (1983), and do not require mass-to-light ratios. In this way, Eq. 4 can clearly be seen to be a sum of gradients, as is the dark matter RC formula in the next section.

### 2.2. Dark matter rotation curve fitting formula

The dark matter rotation curve (RC) formula is

$$v(r)_{rot}^2 = v(r)_{lum}^2 + v(r)_{dm}^2, \quad (6)$$

where terms in  $v(r)_{lum}$  are the Keplerian velocity predictions in Eq. 5,  $v(r)_{dm}$  are the velocities attributed to dark matter, and terms in  $v(r)_{rot}$  are the model prediction which are fitted to the RC velocities  $v(r)_{obs}$  in Eq. 1 from shifted spectra. All velocities are assumed to be those of test particles in circular orbits, in the plane of the stellar disk, about the rotation axis of the galaxy at  $r = 0$ .

### 2.3. Radial Acceleration Relation

The Radial Acceleration Relation (RAR) is an empirical relation (McGaugh et al. 2016) which has been considered as the phenomenological basis for MOND (Dutton et al. 2019; Desmond et al. 2023), though it has a simpler functional form and less scatter. For this reason, we use the RAR fits in comparison to RCFM and dark matter fits in this paper.

The RAR approaches rotation curves from the same MONDian paradigm of a changing law of inertia, but has been shown to be consistent with dark matter fits on a sample of simulated galaxies (Keller & Wadsley 2017).

In the RAR, the changing acceleration scale is a free parameter represented by  $g_{\dagger}$

$$g_{obs} = \frac{g_{bar}}{1 - e^{-(\sqrt{g_{bar}/g_{\dagger}})}} \quad (7)$$

for  $g_{bar}$  the radial acceleration due to the estimated total baryons and  $g_{obs}$  is the model prediction fitted to the flat-rotation curve velocities from Doppler shift. All terms in  $g$  are gradients in the potential as in Eq. 4.

#### 2.4. New rotation curve fitting model (RCFM)

The physical paradigm for the new rotation curve fitting model (RCFM) is: the luminous mass is the only mass, the velocity  $v_{lum}$  due to the baryons is the only velocity, and excesses in Doppler shifted spectra represented by the “flat” rotation velocities  $v_{obs}$  are due to relative frame effects from the Milky Way galaxy. For clarity in what follows, we now drop explicit functional dependence on  $r$ . All terms can be assumed to be evaluated one-to-one in radius between the galaxy being observed and the Milky Way, with the exception of the model’s free parameter  $\alpha$  which is single valued for each galaxy fitted. Constants like Newton’s  $G$  and the speed of light  $c$  will be set to 1.

We construct the heuristic new rotation curve fitting formula by replacing the dark matter contribution  $v_{dm}^2$  to the rotation curve in Eq. 6 with two Lorentz-type maps  $S_1$  and  $S_2$  which represent the frame-dependent effects due to the Milky Way;

$$v_{rc}^2 = v_{lum}^2 + \alpha \kappa^2 S_1 S_2. \quad (8)$$

Terms in  $\kappa$  are a measure of relative curvature

$$\kappa = \frac{\Phi_{gal}}{\Phi_{mw}}. \quad (9)$$

This prescription is an implicit assumption that contributions to Doppler shifted spectra from translation ( $v_{lum}$  in Eq. 5) and from relative curvature ( $S_1 S_2$ ) are roughly separable as in Eq. 8 (Jackson 1999).

The RCFM galaxy maps  $S_1$  and  $S_2$  (Eq. 8) are constructed from the tetrad formalism of general relativity (Tecchioli 2019), where an inertial frame field metric (Minkowski  $\eta^{ab}$ ) can be attached to any point on a curved manifold. The frame fields  $e_a^\mu$  are related to the curved spacetime metric  $g^{\mu\nu}$  in the following way

$$g^{\mu\nu} = e_a^\mu e_b^\nu \eta^{ab}. \quad (10)$$

In the frame field formalism “when going from one local inertial frame at a given point to another at the same point, the fields transform with respect to a Lorentz transformation” (Jetzer 2017). Our goal then, is to use Lorentz-type functions to map the target galaxies onto the Milky Way one-to-one in radius, using the weak-field Schwarzschild time coefficients  $g_{00} = -(1 - 2\Phi)$  to characterize the clock field which defines the effects on photon frequency. The weak-field timelike Schwarzschild field frames are defined by

$$e_0^0 = \sqrt{1 - 2\Phi}. \quad (11)$$

Terms in  $\Phi$  are the Newtonian gravitational potential (Wald 1984). Classically, the  $\Phi$  of galaxies are integrated from the large  $R$  limit of the data with a boundary value of  $\Phi = 0$ , into a negative maxima at the small  $r$  limit (Eq. 2). This is an implicit assumption of a globally flat embedding space, which ensures that the potential goes to zero at a distance of infinity from the mass distribution. Recent observations (Pomarède et al. 2020), however, have shown that on the relevant length scales of galaxies and groups of galaxies we have not recovered flat spacetimes. In fact, the external environments of galaxies and flowlines of groups of galaxies are exceedingly complex and diffusely populated with matter, demonstrating structure with sources and sinks. In addition, the value of the vacuum energy remains an outstanding physics problem (Zel’dovich 1968). In the absence of definite knowledge of the values of  $\Phi$  at the large  $r$  limit of individual galaxies, and since all RCFM terms are ratios of terms in  $g_{00}$  for two galaxies, we instead inform the integration of the gravitational potentials from Wolfgang Rindler’s statement that “the center of each galaxy provides a basic local standard of nonacceleration ... so then can be treated like a local inertial frame relative to its own center” (Rindler 2013).

From Rindler's insight, we compare galaxies as inertial frames from their centers. In practice, galaxy potentials are summed from  $\Phi = 0$  at  $r \approx 0$  out to a positive, constant value at the large  $R$  limit of the data. This is an implicit assumption that all curvatures are all the same at galaxy centers. This produces positive definite gravitational potentials, which are subtracted from 1 in the clock term  $g_{00} = -(1 - 2\Phi)$ . Gravitational potentials calculated in this way obey Poisson's equation Eq. 3 and the central force law Eq. 4, but allow for a non-flat embedding space with no loss of generality.

The curved 2-frame mapping  $S_1$  is

$$S_1 = \sinh \zeta, \quad (12)$$

with a rapidity defined by

$$e^\zeta = \sqrt{\frac{g_{00}|_{gal}}{g_{00}|_{mw}}}, \quad (13)$$

for  $g_{00}|_{gal}$  representing the target galaxy and  $g_{00}|_{mw}$  the Milky Way. A cartoon of the  $S_1$  transformation is represented in Fig. 1

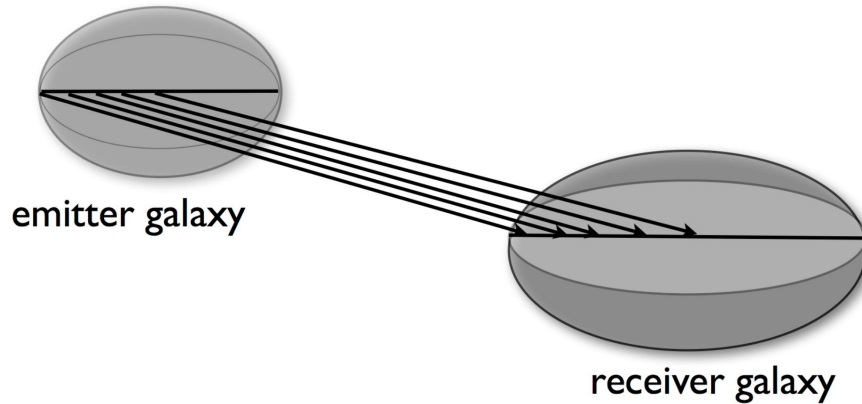


**Figure 1.** Curved 2-frame mapping  $S_1$

The second transformation is

$$S_2 = \cosh \tau \quad (14)$$

for the rapidity angle  $\tau$  defined by

$$e^\tau = e^{(\zeta+\eta)}, \quad (15)$$

for  $e^\tau$  the convolution of the curved 2-frame  $e^\zeta$  (Eq. 13) with the flat 2-frame  $e^\eta$

$$e^\eta = \sqrt{\frac{1+\beta}{1-\beta}}. \quad (16)$$

Terms in  $\beta = v_{lum}/c$  are the Keplerian velocities estimated from photometry of the luminous mass. This last step is necessary because observations are made in locally flat frames, where the metric is Minkowski  $\eta^{\alpha\beta}$ . The Keplerian velocities in Eq. 16 are our best estimate of flatness, as evidenced by the fact that dark matter is not required to reproduce the RC of our Solar System.

Previously, Rindler extended the transforms of special relativity to accelerated frames on a flat background (Boyer 2011); viewed as Rindler’s accelerated coordinates,  $S_1$  is timelike and  $S_2$  is spacelike (Misner et al. 1973; Wald 1984; Rindler 2013). A cartoon of the  $S_2$  transformation is represented in Fig. 2

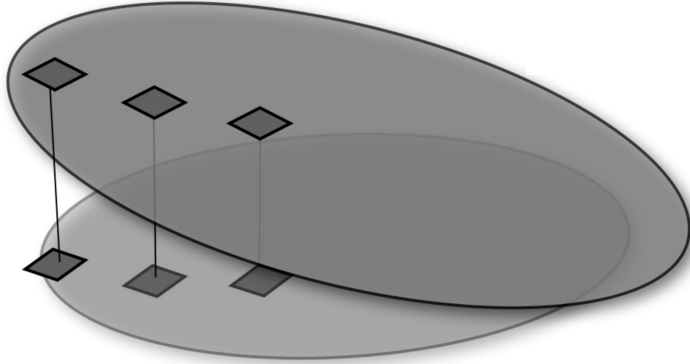


**Figure 2.** Mapping from curved 2-frame to flat 2-frame by  $S_2$  transformation

### 2.5. Geometric simplifications

Population synthesis models commonly assume spherical symmetry for the stellar bulge and gas halo, but axial symmetry for the stellar disk (Schwarzschild 1954; Freeman 1970). However, it is a common calculational tool to use spherical symmetry for the entire integrated potential of the luminous mass distribution (Bekenstein 2004; McGaugh 2008; Mistele et al. 2022) because numerical integration of the thin disk is computationally intensive, requiring assumptions of underconstrained boundary conditions and relevant physical scales, which therefore add extra free parameters to the problem (Huré & Hersant 2011). We use the Schwarzschild metric as it is the simplest spherically symmetric representation, which captures the relevant physics of the problem without excess computations. A more detailed analysis could use the interior Schwarzschild metric. We have previously tested the Kerr metric in this context (Cisneros et al. 2015), and found the difference from Schwarzschild predictions are below the observational limits.

Gravitational potentials calculated in a spherically symmetric geometry converge to those in an exponential disk geometry at lengths greater than one-third of the exponential scale-length  $R_e$ , ie.  $r > R_e/3$  (Chatterjee 1987). Since this is the region where dark matter effects becomes important (van Albada et al. 1985), for proof of concept this calculational technique is acceptable. However, in the region from  $r \approx 0$  to  $R_e/3$ , where the RCFM begins to compare galaxies, the spherical assumption overestimates the potential by a factor of  $\approx 2$ . This artifact can be seen in the RCFM results in Tables 11 and 11. Implementation of a thin disk geometry would resolve this artifact of the analysis (de Vaucouleurs 1959),(Freeman 1970), though at significant computational expense.

## 3. DATA

### 3.1. SPARC galaxies

We fit the Spitzer Photometry and Accurate Rotation Curves (SPARC) dataset of 175 nearby galaxies with extended RC data from atomic hydrogen (HI) and H- $\alpha$  (Lelli et al. 2016). HI provides the most reliable RCs because it is dynamically cold, traces circular orbits, and can be observed several effective radii past the stellar disk. This sample of rotationally supported galaxies spans the widest range of masses and morphologies presently available.

These galaxies are accompanied by Keplerian velocities which represent the baryonic mass model from PSM, based on Spitzer Photometry in the near infrared at  $3.6\mu m$ . Near infrared is currently believed to be the best tracer of stellar mass in population synthesis models (PSM) (Schombert et al. 2018), as at this wavelength, mass-to-light ( $\gamma_i$ ) ratios are believed to be almost constant and independent of star formation history (Bell & de Jong 2001; Schombert

**Table 1.** Milky Way Models

Both Milky Way models are replaced from 9.5 to 26.5 kpc with *Gaia* DR3 (Jiao, Yongjun et al. 2023) data.

Author	scale length bulge/bar	Model for the extended RC	Range
Sofue-Xue Sofue (2013); Xue et al. (2008)	0.5 kpc bulge	NFW (Navarro et al. 1996) dark matter	[0,60] kpc
McGaugh McGaugh (2008)	2.0 kpc bar	MOND (Milgrom 1983)	[0,150] kpc

et al. 2018). The SPARC database reports mass-to-light ratios of  $\gamma_i = 1$  in units of  $M_\odot/L_\odot$  at  $3.6\mu m$ . Gas fractions  $v_{gas}$  are calculated from surface density profiles of HI with the formalism given in (Casertano 1983) and scaled by a factor 1.33 to account for cosmological helium abundances. Contributions from molecular gas are ignored because CO data are not available for most SPARC galaxies. Error on these velocities is estimated at 20% (Lelli et al. 2016). The SPARC database can be found at <http://astroweb.cwru.edu/SPARC/>.

### 3.2. Milky Way Luminous Mass Models

The RCFM, as currently formulated, requires a static choice of a luminous mass distribution for the Milky Way. Determining the luminous mass profile of the Milky Way (MW) is an under-constrained problem, due to our observing position from within the galactic disk (Fich & Tremaine 1991). In this paper, we compare two different Milky Way baryon models to the SPARC sample; one from McGaugh (McGaugh 2008) and one from Sofue (Sofue 2013).

The two MW models differ markedly in the inner 7 kpc; as the McGaugh MW has a triaxial bar-bulge and the Sofue MW has a de Vaucouleurs bulge. The Sofue MW model is used from 0 to 20 kpc, and extended with the Xue MW model from 20 to 60 kpc Xue et al. (2008). The Sofue and Xue MW models come from the same data and a dark matter model is used for the extended rotation curve. The McGaugh Milky Way model covers from 0 to 150 kpc, and comes from data and the MOND model is used for the extended rotation curve.

From the recent *Gaia* data release (DR3), Jiao, Yongjun et al. (2023) find a Keplerian decline of the rotation curve of the Milky Way in the range of 9.5 to 26.5 kpc, consistent with the RCFM heuristic picture. The ESA *Gaia* mission, taking measurements from the second Lagrange point, has revolutionized the science of the MW with unprecedented detail, statistical accuracy, and a drastic reduction in systematic uncertainties. We have replaced the McGaugh and Sofue-Xue Milky Way model velocities in the range from 9.5 to 26.5 kpc with the Jiao Milky Way velocities, and then shifted the two sides of the given MW models by a constant amount to match the endpoints of the Jiao velocities. See Table 1 for details.

## 4. ANALYSIS AND RESULTS

### 4.1. Fitting procedure

To fit galaxies in the SPARC sample with the RCFM model, the fitting procedure is as follows. First, a Milky Way model is chosen (Sec. 3.2) and the data read in as  $v_{lum}$  for a series of measurements in radii. The galactic gravitational potential is computed as described (see Sec. 2.4), by numerically integrating

$$\Phi(r) = \int_{inner}^{outer} dr \frac{v(r)_{lum}^2}{r}. \quad (17)$$

Once the MW potential is calculated, it remains static for the rest of the fitting procedure.

The data for the galaxies being observed include several pieces of information: the RC velocities  $v_{obs}$  from Doppler shifted spectra, the uncertainty on that measurement  $v_{err}$ , and the components of the luminous mass interpreted as orbital velocities,  $v_{bulge}$ ,  $v_{disk}$ , and  $v_{gas}$ . To calculate the baryonic potential for the galaxy in question,  $v_{lum}$  is first computed as per Eq. 5, for  $\gamma_b = 1$  and  $\gamma_d = 1$ . The  $\Phi_{gal}$  associated with that galaxy is then computed as in Eq. 17.

After the  $\Phi$  for the galaxy being studied and the Milky Way have been calculated, the components must be compared at matching values of  $r$ . To match radii,  $\Phi_{MW}$  is interpolated to produce values at the radii reported in the measured RC data  $v_{obs}$  of the galaxy being observed. Any point with a radius larger than the largest radius in the Milky Way model is discarded.

The RCFM prediction is assembled as in Eq. 8, to give a predicted  $v_{rc}$  which is compared to the RC data  $v_{obs}$ . The equations outlined in Section 2 contain free parameters that must be determined for each galaxy fit:  $\alpha$ ,  $\gamma_b$ , and  $\gamma_d$ . The model’s free parameter  $\alpha$  starts from an initial value of  $\alpha = 0.01$ , and mass-to-light parameters from an initial value of 1.00, and then all parameters are allowed to vary freely and to be determined by minimization of the  $\chi^2$ . The `scipy.optimize.curve_fit` utility in Python is used to perform this minimization.

As noted in Section 2, reported gas fractions are fixed at their reported values (HI scaled for Helium abundance by a factor of 1.33 in the SPARC database), though addition of molecular gas could increase mass fractions in the inner kiloparsec of a galaxy (McGaugh 2004).

#### 4.2. Evaluating goodness-of-fits

There are two metrics by which different rotation curve fitting models are compared, the resulting reduced  $\chi_r^2$  values and the mass-to-light ratios. Since error estimates on RC velocities have not been standardized across the field (de Blok et al. 2008a; Gentile et al. 2011),  $\chi_r^2$  values can only be compared when fitted to the same RC data. In Table 11 we compare  $\chi_r^2$  values from three models; dark matter halo, Radial-Acceleration-Relation (RAR) (McGaugh et al. 2016; Lelli et al. 2017; Li et al. 2018) and RCFM, fitted to the SPARC database of galaxy RCs (Lelli et al. 2016). RCFM  $\chi_r^2$  values are remarkably low, providing confidence in the faithfulness of the model to galaxy RC data.

The average mass-to-light ratios from RCFM fits yield bulge mass-to-light ratios which are within the error estimates on population synthesis models (PSM). The RCFM disk mass-to-light ratios are approximately a factor of two larger than PSM, consistent with the artifact introduced from the spherical integration technique, see Sec. 2.5 for a full explanation. This artifact can be removed by including an exponential disk integration.

#### 4.3. Comparing Milky Way models

The RCFM fits require a static choice for the Milky Way baryon distribution. In Table 9 and 10 we compare the RCFM fit results for the two different Milky Way model assumptions used in this paper. As can be seen in the table, for the 36 most reliable galaxies in the SPARC sample the two Milky Way models are equivalent (see Sec. 4.6). However, for the whole SPARC sample of 175 galaxies the RCFM fits using the Sofue-Xue-Jiao Milky Way performs better with an average  $\chi_{red}^2 = 2.39$ , versus those from McGaugh-Jiao Milky Way  $\chi_{red}^2 = 7.09$ . Based on this, values in Table 11 and figures are from RCFM fits assuming the Sofue-Xue-Jiao Milky Way.

The residuals of fits to the SPARC sample are also used to compare the two different MW models (see Sec. 3.2). Histograms of residuals normalized by the error in velocity observations are shown in Fig. 4. In all cases, residuals of model fits to observed velocity data followed a narrow distribution centered at zero with a range of  $\pm 3$  km/s, albeit with heavy tail features. The behavior of the residuals did not vary greatly between MW models, suggesting that the fitting parameters in our model are robust with respect to differing MW model assumptions at this present level of analysis. With a finer grained analysis and a larger sample, the degeneracy between MW models may be resolved.

A Gaussian fit on residuals from fits using the McGaugh-Jiao MW model gave a mean of  $-0.003$  km/s, standard deviation of 0.807 km/s; whereas a Gaussian fit to the residuals from fits using the Sofue-Xue-Jiao MW model gave a mean of  $-0.016$  km/s, standard deviation of 0.802 km/s. The residuals are shown in Fig. 4. The small values associated with these quantities in both cases provide confidence that our fits match data closely.

However, the Gaussian fits did not quite capture the full peak and heavy tails in the residuals. This suggests that there may be non-Gaussian error in the observations of galaxy velocities. To address this, the residuals were also fit to an exponential function shown in Fig. 5. The exponential function captured both the peak and the heavy-tailed behavior of the distributions more faithfully.



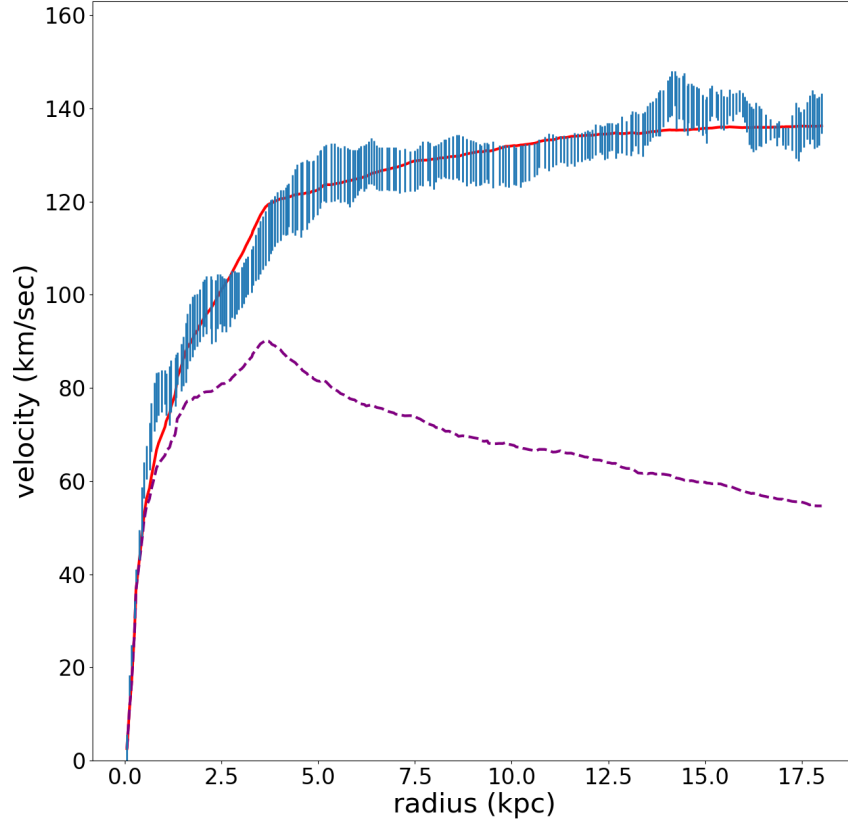


**Figure 3.** NGC 2403 , rotation curve data (blue points with error bars), and RCFM fit (red line) using the baryonic mass model (dashed purple line) from de Blok et al. (2008b) and the Sofue-Xue-Jiao Milky Way model Sofue (2013); Xue et al. (2008); Jiao, Yongjun et al. (2023).

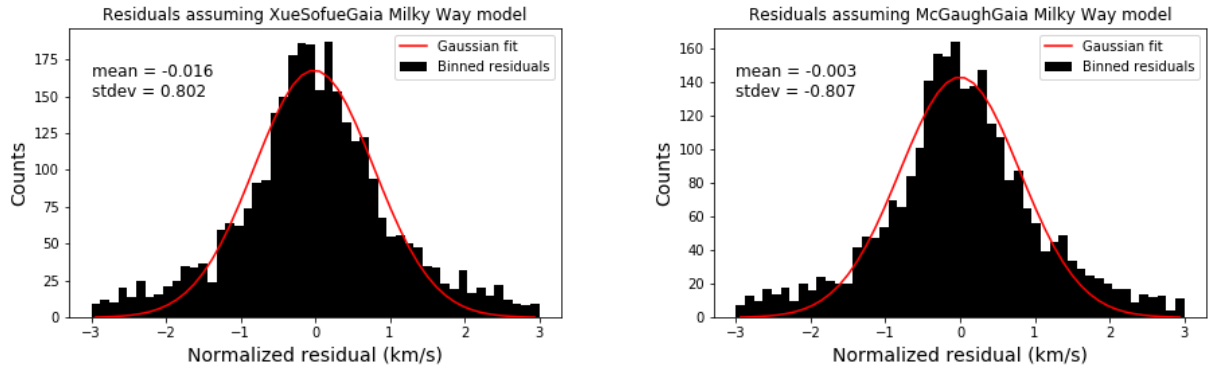


**Figure 4.** Normalized residuals from fits assuming either Sofue-Xue-Jiao or McGaugh-Jiao Milky Way models, fitted by a Gaussian function. The means and standard deviations are shown.

#### 4.4. Individual Galaxy Results

In this section we will compare fit results from the RCFM, RAR and dark matter models for well-studied galaxies. All reported  $\gamma_i$  in what follows are in units of solar mass per solar luminosity  $M_{\odot}/L_{\odot}$ .

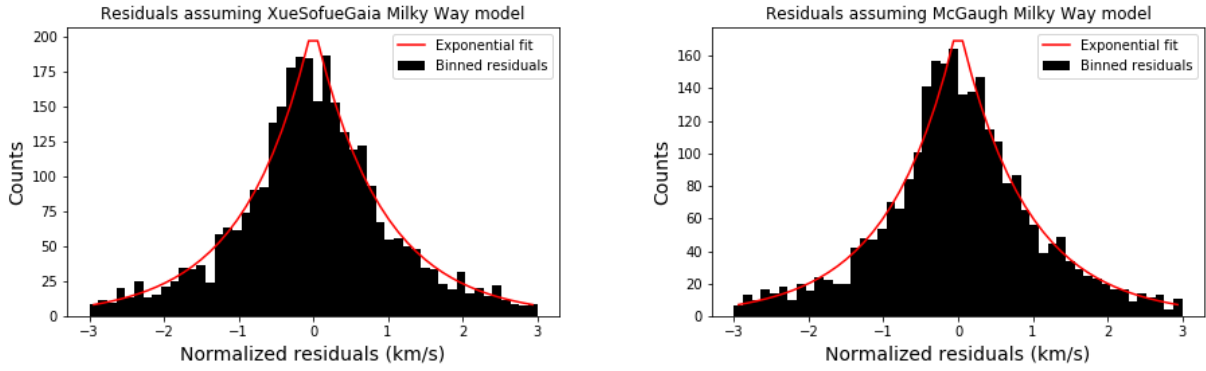


**Figure 5.** Normalized residuals from fits assuming either Sofue-Xue-Jiao or McGaugh-Jiao Milky Way models, fitted by an exponential function.

#### 4.4.1. NGC 2841

NGC 2841 is a star dominated, flocculent spiral galaxy, which historically has been regarded as a problematic case for MOND ((Gentile et al. 2011)). RAR finds a good fit for this galaxy after adjusting the Cepheid distance of 14.1 Mpc, by  $1\sigma$ , to 15.5 Mpc. Cepheid variable stars are the most accurate distance indicators currently available. The RCFM fit is shown in Fig. 6 at the Cepheid based distance, and fit results are compared to dark matter and RAR in Table 2.

**Table 2.** NGC 2841

	Model	$\gamma_d$	$\gamma_b$	$\chi_R^2$	distance(Mpc)
	Dark Matter Iso	0.60	0.66	1.58	14.1
	RAR	0.81	0.93	1.52	15.5
	RCFM	0.91	1.10	1.36	14.1

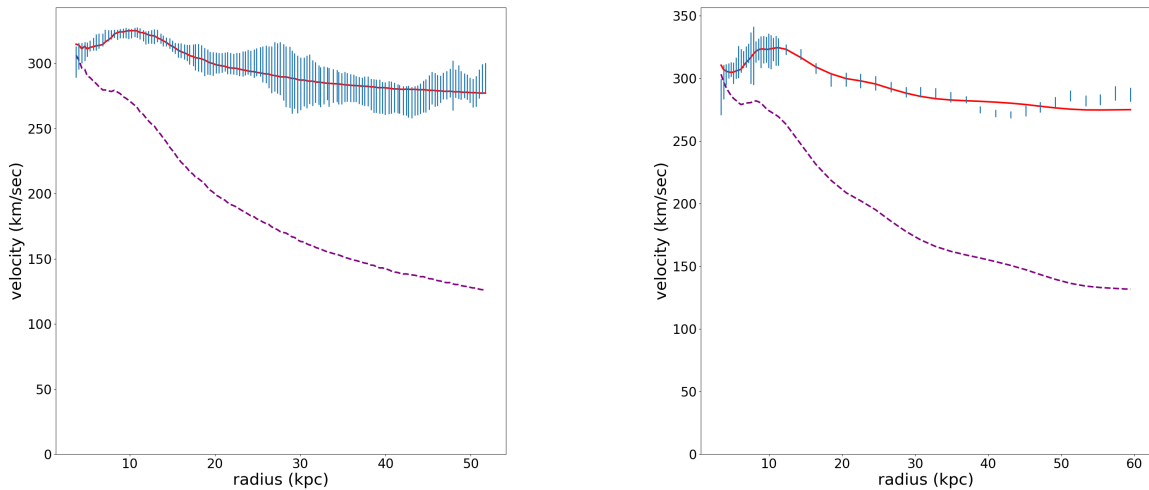


**Figure 6.** NGC 2841 RCFM fits (both figures). Lines are as in Fig. 3. (Left Figure) RC data and baryonic mass model from (de Blok et al. 2008b). (Right Figure) RC data and baryonic mass model from (Lelli et al. 2016).

## 4.4.2. IC 2574

IC 2574 is a dwarf spiral galaxy, dominated by gas with no central stellar bulge. RAR finds a good fit to this galaxy but adjusts the distance and inclination by 1 to  $1.5\sigma$ . This galaxy is problematic for dark matter model fits, as the model overestimates the inner RC out to 10 kpc (Navarro et al. 2017). RCFM fits this galaxy successfully, at the reported tip of the red giant branch distance of 3.91 Mpc, Fig.7, model comparisons are in Table 3.

**Table 3.** IC 2574

	Model	$\gamma_d$	$\gamma_b$	$\chi_r^2$
	Dark Matter Iso	0.77	–	2.51
	RAR	0.07	–	1.44
	RCFM	1.10	–	2.27

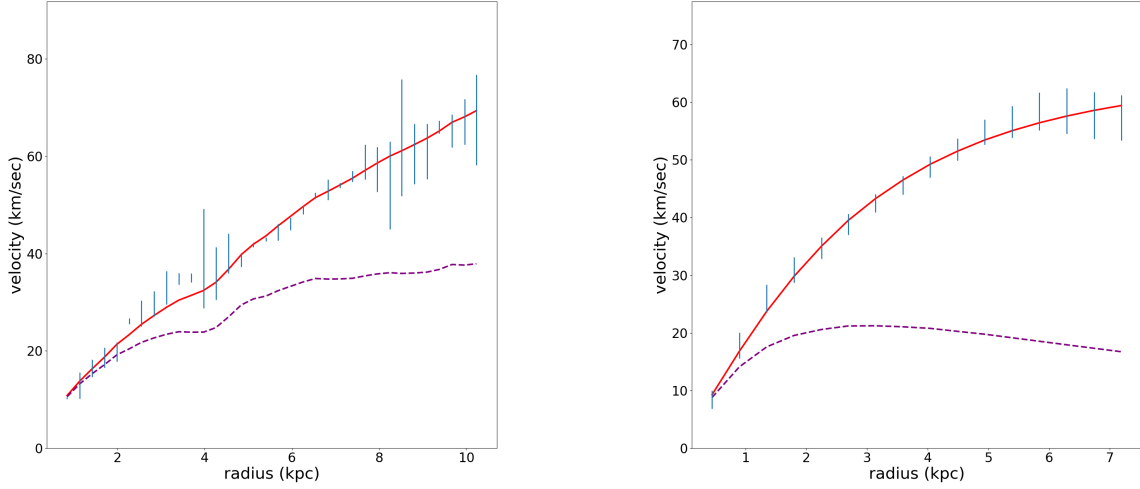


**Figure 7.** IC 2574 (left) and D 631-7 (right). RCFM fits to gas dominated dwarf galaxies. RC and baryon models from (Lelli et al. 2016). Lines are as in Fig. 3.

## 4.4.3. NGC 3198

NGC 3198 is a barred spiral in Ursa Major, which has been well studied. It has been considered a problem galaxy for MOND, when the distance is a free parameter in fits (Gentile et al. 2011), as the preferred MOND distance is  $2\sigma$  different from that reported from Cepheids. However, in the SPARC database the RAR fit to this galaxy at the Cepheid distance reproduces the RC well. This galaxy has no bulge component, as indicated in Table 4. See Fig. 8 for the RCFM fit.

**Table 4.** NGC 3198

	Model	$\gamma_d$	$\gamma_b$	$\chi_r^2$	distance (MPC)
	Dark Matter Iso	0.52	–	1.31	13.7
	RAR	0.77	–	2.06	13.8
	RCFM	0.88	–	1.72	13.8

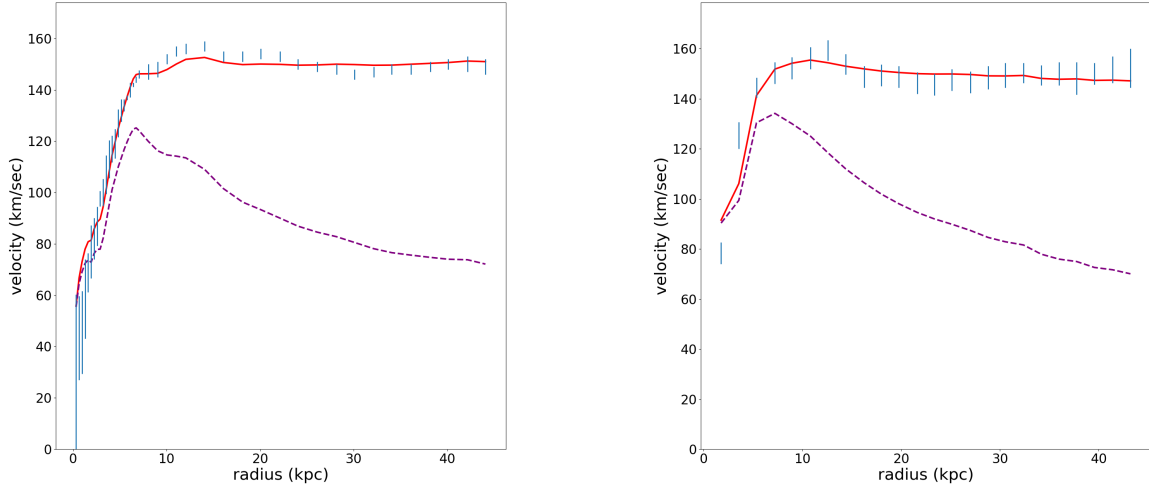


**Figure 8.** RCFM fits to NGC 3198. Left figure, RC and baryon model from (Lelli et al. 2016). Right figure, RC and baryon models from (Gentile et al. 2013). Lines are as in Fig. 3.

#### 4.4.4. NGC 7814 and NGC 891

The spiral galaxies NGC 7814 and NGC 891 present an interesting challenge to dark matter and MOND models. Both galaxies are presented edge-on on the sky, and both have essentially identical RCs, but are extreme opposites in morphologies. NGC 7814 is a bulge dominated galaxy and NGC 891 is almost entirely a disk galaxy. Fraternali et al. (2011) asks “why are these RCs so identical if their dark matter halos are necessarily different to accommodate the differences in the luminous mass?”

In the RCFM paradigm the two RCs are very similar in magnitude, but differ in their inflections at large radii; NGC 7814 inflects up, whereas NGC 891 inflects down. RCFM fits to these galaxies are successful, see Fig.9 and Tables 5 and 6. We report here fits to the (Fraternali et al. 2011) RC data included in the SPARC database.

**Table 5.** Bulge dominated NGC 7814

	Model	$\gamma_d$	$\gamma_b$	$\chi_r^2$
	Dark Matter Iso	0.68	0.71	0.39
	RAR	1.17	0.52	1.334
	RCFM	0.38	0.68	0.63

**Table 6.** Disk dominated NGC 891

	Model	$\gamma_d$	$\gamma_b$	$\chi_r^2$
	Dark Matter Iso	0.77	1.63	1.30
	RAR	0.32	—	25.16
	RCFM	0.66	—	1.89

#### 4.4.5. NGC 5055

In this section we compare two different sets of NGC 5055 RC data from HI, and their resulting dark matter, RAR and RCFM fits. The first RC is from (Battaglia et al. 2006) as reported in SPARC. Their luminous model has no stellar bulge. The RC data and luminous mass model are reported at the reliable distance of  $9.83 \pm 0.30$  Mpc, from the Tip of The Red Giant Branch method.

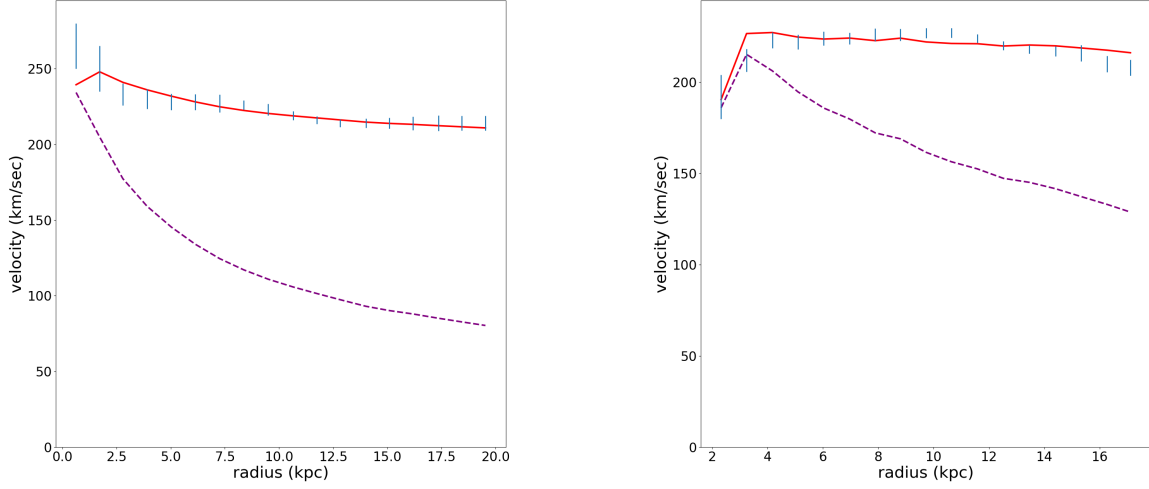


**Figure 9.** Bulge dominated NGC 7814 (left) and disk dominated NGC 891 (right). RCFM fits comparison of two similar RC with very different luminosity profiles. RC and baryon models for both are from (Lelli et al. 2016). Lines are as in Fig. 3.

**Table 7.** Results for a disk dominated NGC 5055, RC data and mass model from SPARC (Battaglia et al. 2006).

	Model	$\gamma_d$	$\gamma_b$	$\chi_r^2$
	Dark matter - Isothermal Halo	0.26	-	6.19
	RAR	0.56	-	7.42
	RCFM	0.62	-	6.29

The second RC for NGC 5055 is from the THINGS (de Blok et al. 2008a) at a distance of 10.1 Mpc from the Hubble Flow, including a stellar bulge component. RCFM fits to both sets of RC data can be seen in Fig.10, at reported distances, using the reported luminous mass models. This galaxy serves as an example of the under-constrained nature of galaxy mass modeling (Conroy et al. 2009). Details of the fits are given in Table 10.

**Table 8.** Results for a bulge dominated NGC 5055. RC data and mass model from (de Blok & McGaugh 1997).

	Model	$\gamma_d$	$\gamma_b$	$\chi_r^2$
	Dark Matter Iso	0.79	0.11	8.13
	Dark Matter NFW	0.79	0.11	10.31
	RAR	0.43	0.46	2.63
	RCFM	0.57	0.23	1.30

#### 4.5. Galaxies for which model fits fail

Quality flag ( $Q$ ) are assigned in the SPARC galaxy database, using the following scheme:  $Q = 1$  for galaxies with high-quality HI data or hybrid  $H\alpha$ /HI rotation curves;  $Q = 2$  for galaxies with minor asymmetries and/or HI data of lower quality;  $Q = 3$  for galaxies with major asymmetries, strong non-circular motions, and/or offsets between HI and stellar distributions. They state galaxies with  $Q = 3$  are not suited for detailed dynamical studies. Of the three models compared in this paper for the 175 SPARC galaxies;

- The RAR fits all galaxies;
- The RCFM fits 172 galaxies; fits fail for UGC06628 ( $Q = 2$ ), and F561-1, UGC04305 ( $Q = 3$ ),

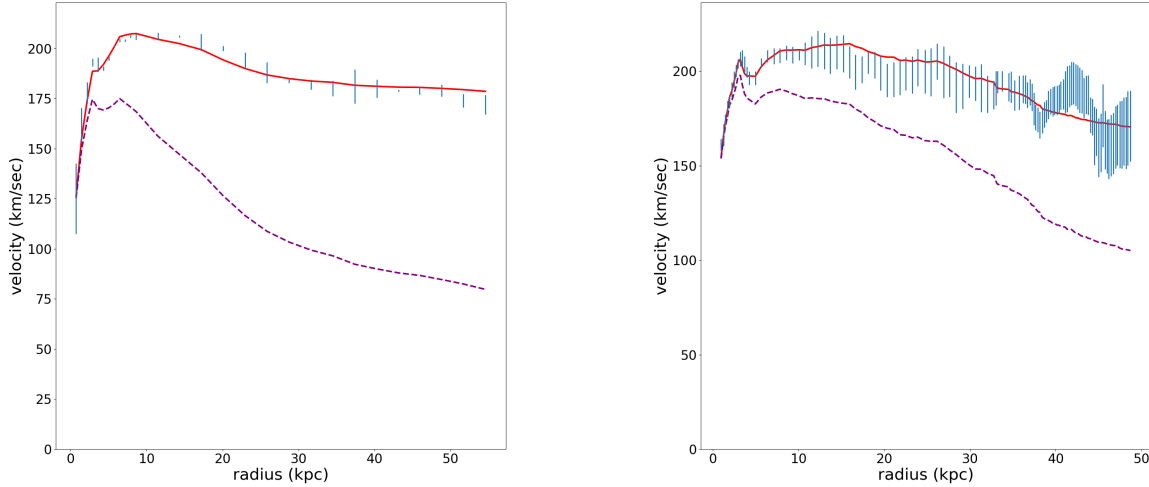


**Figure 10.** RCFM comparison fits for NGC 5055. Left figure RC and baryon model are from (Lelli et al. 2016). Right figure RC and baryon model are from (de Blok et al. 2008b). Lines are as in Fig. 3.

- The dark matter model fits 165 galaxies; fits fail for D512-2, UGC00634, NGC6789, UGC00891, UGC02023, UGC05999, UGC07232 and UGC09992 ( $Q = 2$ ), and F567-2 and F574-2 ( $Q = 3$ ).

#### 4.6. Free Parameter Correlation

We test a correlation between the model’s free parameter  $\alpha$  and a ratio of total luminosity  $L_{total}$  by the half-light radius  $R_{eff}$  (effective radius). To test this correlation, we first create a subset of galaxies from the SPARC dataset by the following selection criteria:

1. Select galaxies with the most accurate and reliable distance estimates (tip of the red giant branch and Cepheid variable stars), rejecting all other galaxies.
2. Select galaxies with inclinations on the sky in the range of  $15^\circ$  to  $80^\circ$ , rejecting galaxies with an inclination greater than  $80^\circ$  as difficult to assign a true surface brightness profile, and those at inclinations less than  $15^\circ$  as being difficult to report line of sight Doppler shifts accurately.
3. Exclude galaxies with quality factor  $Q = 3$  as not suited to dynamical studies due to asymmetries, non-circular motions, and/or offsets between stars and gas, using assigned SPARC  $Q$  factors as in (Lelli et al. 2016).

By this process, a training set of 36 galaxies are selected, as reported in Table 9. We then plot the subset’s  $\alpha$  values versus the ratio of  $L_{total}/R_{eff}$ , and fit the distribution with a power law as shown in Fig. 11. The total luminosity and effective radii numbers used are as reported in the SPARC database. Luminosity measurements are taken in the wavelength of  $3.6\mu m$ , assuming a solar absolute magnitude of 3.24 at  $3.6\mu m$  (Oh et al. 2008) in units of  $10^9$  solar  $L_\odot$ . As can be seen in in Fig. 11 the subset appears to be highly correlated to the ratio of photometric quantities, though slightly different functionally for the choice of Milky Way.

## 5. CONCLUSIONS

At this time, there are many discrepancies between cosmology theory and observations which are resolved by dark matter models (Sanders 2010; Tully et al. 2014; Naidu et al. 2022). In this paper we address only one such discrepancy, the flat-rotation curve problem of spiral galaxies. This choice is due to the clear symmetry presented in the rotation curve data. Other dark matter problems require cosmological model assumptions, beyond the scope of the current paper.

**Figure 11.** RCFM free parameter  $\alpha$  vs. a ratio of total luminosity by effective radius, for a subset of (36) SPARC Galaxies with the best distance estimates, as listed in Table 9.

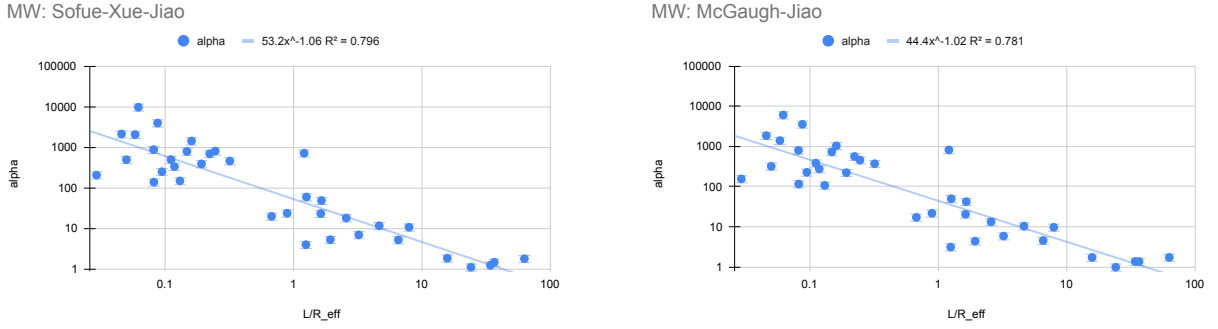


**Table 9.** Training Set — Average Results<sup>a</sup>

Model	$\gamma_d$	$\gamma_b$	$\chi_{red}^2$
RAR	0.46	0.74	3.89
RCFM (MW: Sofue-Xue-Jiao)	1.04	0.87	1.60
RCFM (MW: McGaugh-Jiao)	1.00	0.87	1.65
Dark Matter	0.50	0.66	1.59

<sup>a</sup> The averages do not reflect target galaxies which fail to fit; in this subset RCFM and RAR have no galaxies which fail, the dark matter model (Isothermal halo) has two which fail (NGC6789, UGC07232). The average stellar mass-to-light ratios  $\gamma_i$  are in units of solar mass per solar luminosity  $M_{\odot}/L_{\odot}$ .

Here we reinterpret the flat-rotation curve problem not as a problem of missing mass but rather, at the level of the data, as a problem of relative frame effects due to our home galaxy. We predict that the flat-rotation curve problem is an artifact of misinterpretation of Doppler shifted spectra from external galaxies, removing the need for dark matter halos on galaxies. This framing places primary importance on the role of the Milky Way, and compactly explains both why the Milky Way sits roughly at the inflection point in the Universal Rotation Curve spectrum of 1,100 galaxies (Persic et al. 1996) and why MOND is both successful and limited.

The rotation curve fitting model (RCFM) presented here reproduces the fitting successes of MOND, RAR (Radial Acceleration Relation) and dark matter models on a sample of 175 well studied galaxy rotation curves (Lelli et al. 2016), but does not modify classical physics. We emphasize that the only input to the RCFM is the luminous mass. Independent of the interpretation of the various quantities appearing in the formulae presented in this paper, this is a one parameter fit to the data. What is more, the RCFM free parameter is highly correlated with a ratio of observable photometric parameters. Our results are presented in this paper in comparison to dark matter and RAR results for the same galaxies, from the SPARC sample of 175 rotation curves (Lelli et al. 2016). RAR has a simpler functional form, though the same physics paradigm, as MOND. The recent *Gaia* DR3 data release Jiao, Yongjun et al. (2023) has shown that the rotation curve of the Milky Way demonstrates a Keplerian decline from 10 - 26.5 kpc, consistent with the RCFM model paradigm presented here. The upcoming Large Survey of Space and Time at the Vera C. Rubin Observatory (Željko Ivezić et al. 2019) can falsify this model if the Milky Way rotation curve beyond 26.5 kpc is found to require a dark matter halo.

## 6. ACKNOWLEDGMENTS

This work is dedicated to Emmett Till. We acknowledge and express gratitude to the first nations peoples on whose unceded lands this was written; including but not limited to the the Coast Salish bands of the Puget Sound, the Cheyenne, Arapaho and Southern Ute Peoples of Colorado, and the Algonquian and Iroquoian Peoples of Massachusetts and New York, and the Navajo Peoples of New Mexico. The authors would like to thank V. P. Nair, T. Boyer, I. Chavel, R. Waltherbos, N. P. Vogt, S. McGaugh, A. Klypin, T. Quinn, S. Tuttle, M. Juric, R. Rivera, N. Oblath, J. Formaggio, J. Conrad, P. Fisher, Y. Sofue, C. Mihos, and M. Merrifield.

**Table 10.** Training Set from SPARC galaxies

Galaxy Name	MW: M.J. <sup>a</sup> $\chi_{red}^2$	MW: S.X.J. <sup>b</sup> $\chi_{red}^2$	Distance (Mpc)	Distance Method <sup>c</sup>	Inc (deg)
CamB	0.52	0.36	3.36	2	65
D564-8	0.03	0.07	8.79	2	63
D631-7	0.52	0.36	7.72	2	59
DDO154	8.65	8.66	4.04	2	64
DDO168	4.17	4.12	4.25	2	63
ESO444-G084	1.23	0.63	4.83	2	32
IC2574	1.88	2.05	3.91	2	75
NGC0024	0.82	0.80	7.3	2	64
NGC0055	2.24	2.40	2.11	2	77
NGC0247	2.26	2.24	3.7	2	74
NGC0300	0.41	0.41	2.08	2	42
NGC2403	12.05	11.52	3.16	2	63
NGC2683	0.95	0.97	9.81	2	80
NGC2841	1.51	1.35	14.1	3	76
NGC2915	0.62	0.58	4.06	2	56
NGC2976	0.45	0.46	3.58	2	61
NGC3109	0.30	0.27	1.33	2	70
NGC3198	1.42	1.50	13.8	3	73
NGC3741	0.76	0.63	3.21	2	70
NGC4214	1.55	1.32	2.87	2	15
NGC5055	6.29	6.10	9.9	2	55
NGC6503	1.14	1.14	6.26	2	74
NGC6789	0.86	0.94	3.52	2	43
NGC6946	2.08	1.98	5.52	2	38
NGC7331	1.08	1.09	14.7	3	75
NGC7793	0.72	0.72	3.61	2	47
UGC04483	0.38	0.44	3.34	2	58
UGC07232	1.07	1.02	2.83	2	59
UGC07524	1.40	1.41	4.74	2	46
UGC07559	0.17	0.20	4.97	2	61
UGC07577	0.06	0.06	2.59	2	63
UGC07866	0.08	0.07	4.57	2	44
UGC08490	0.15	0.13	4.65	2	50
UGC08837	0.62	0.65	7.21	2	80
UGCA442	0.74	0.73	4.35	2	64
UGCA444	0.10	0.10	0.98	2	78

<sup>a</sup> Milky Way:M.J. is McGaugh-Jiao<sup>b</sup> Milky Way:S.X.J. is Sofue-Xue-Jiao<sup>c</sup> Distance method: 2 = tip of the red giant branch, 3 = Cepheids. Distance and inclination information from (Lelli et al. 2016).



Table 11. Fits to the SPARC galaxies RCs

MW: SXJ	DM	DM	DM	RCFM	RCFM	RCFM	RAR	RAR	RAR	
Galaxy	$\chi_r^2$	$\gamma_{disk}$	$\gamma_{bulge}$	$\chi_r^2$	$\gamma_{disk}$	$\gamma_{bulge}$	$\chi_r^2$	$\gamma_{disk}$	$\gamma_{bulge}$	Q
Averages:	1.90	0.51	0.11	2.39	1.13	0.78	4.22	0.64	0.73	–
CamB	2.99	0.34	0.00	0.23	0.00	...	5.76	0.34	...	2.00
D512-2	NAN	0.50	0.00	0.21	1.48	...	0.37	0.48	...	2.00
D564-8	0.26	0.49	0.00	0.11	1.21	...	3.16	0.40	...	2.00
D631-7	0.85	0.40	0.00	0.30	0.26	...	15.87	0.20	...	1.00
DDO064	0.48	0.51	0.00	0.45	1.58	...	0.33	0.48	...	1.00
DDO154	3.23	0.41	0.00	10.58	1.18	...	3.48	0.19	...	2.00
DDO161	0.36	0.50	0.00	0.62	0.97	...	1.47	0.23	...	1.00
DDO168	6.03	0.45	0.00	4.36	0.76	...	19.71	0.46	...	2.00
DDO170	2.45	0.49	0.00	3.19	1.84	...	4.92	0.79	...	2.00
ESO079-G014	1.61	0.51	0.00	3.86	1.09	...	4.33	0.50	...	1.00
ESO116-G012	1.27	0.55	0.00	1.03	1.04	...	2.44	0.35	...	1.00
ESO444-G084	2.74	0.51	0.00	0.40	1.86	...	3.25	0.42	...	2.00
ESO563-G021	12.37	0.55	0.00	16.41	1.00	...	28.84	0.43	...	1.00
F561-1	1.14	0.50	0.00	NAN		...	1.56	0.52	...	3.00
F563-1	0.70	0.50	0.00	0.95	2.06	...	1.50	0.56	...	1.00
F563-V1	0.98	0.50	0.00	0.29	0.99	...	0.88	0.48	...	3.00
F563-V2	0.47	0.51	0.00	0.11	2.20	...	0.99	0.59	...	1.00
F565-V2	0.16	0.50	0.00	0.31	2.22	...	0.47	0.50	...	2.00
F567-2	NAN	0.50	0.00	0.50	1.31	...	2.20	0.56	...	3.00
F568-1	0.18	0.50	0.00	0.72	1.91	...	1.29	0.61	...	1.00
F568-3	1.18	0.47	0.00	1.79	1.31	...	3.06	0.41	...	1.00
F568-V1	0.19	0.51	0.00	0.14	2.14	...	1.04	0.81	...	1.00
F571-8	0.75	0.37	0.00	2.04	0.17	...	41.61	0.11	...	1.00
F571-V1	0.18	0.52	0.00	0.20	1.49	...	0.29	0.50	...	2.00
F574-1	0.35	0.48	0.00	1.42	1.54	...	2.50	0.71	...	1.00
F574-2	NAN	0.48	0.00	0.19	0.75	...	0.09	0.49	...	3.00
F579-V1	0.06	0.51	0.00	1.07	1.63	...	2.56	0.63	...	1.00
F583-1	0.36	0.50	0.00	1.04	1.87	...	2.66	0.91	...	1.00
F583-4	0.42	0.51	0.00	0.28	1.30	...	0.13	0.48	...	1.00
IC2574	2.51	0.77	0.00	2.27	1.10	...	1.44	0.07	...	2.00
IC4202	8.67	0.50	0.31	32.72	1.09	0.74	41.91	1.60	0.34	1.00
KK98-251	0.35	0.49	0.00	0.42	1.67	...	1.23	0.44	...	2.00
NGC0024	0.37	0.54	0.00	0.73	1.39	...	0.85	1.01	...	1.00
NGC0055	0.55	0.39	0.00	2.86	1.01	...	1.58	0.19	...	2.00
NGC0100	0.10	0.49	0.00	0.10	0.93	...	1.29	0.28	...	1.00
NGC0247	2.38	0.46	0.00	2.18	1.53	...	3.06	0.78	...	2.00
NGC0289	1.97	0.45	0.00	1.78	0.74	...	2.13	0.92	...	2.00
NGC0300	0.47	0.50	0.00	0.42	1.14	...	0.91	0.40	...	2.00
NGC0801	7.07	0.64	0.00	7.38	0.77	...	7.75	1.33	...	1.00
NGC0891	4.24	0.27	0.60	1.89	0.66	0.00	7.37	0.33	0.40	1.00
NGC1003	2.67	0.77	0.00	3.42	0.77	...	4.67	0.37	...	1.00
NGC1090	1.54	0.53	0.00	2.27	0.81	...	2.78	0.74	...	1.00
NGC1705	0.08	0.49	0.00	0.13	1.25	...	0.37	1.22	...	3.00

Continued on next page

Table 11 – continued from previous page

MW:SXJ	DM	DM	DM	RCFM	RCFM	RCFM	RAR	RAR	RAR	
Galaxy	$\chi_r^2$	$\gamma_{disk}$	$\gamma_{bulge}$	$\chi_r^2$	$\gamma_{disk}$	$\gamma_{bulge}$	$\chi_r^2$	$\gamma_{disk}$	$\gamma_{bulge}$	Q
NGC2366	1.09	0.39	0.00	2.34	1.06	...	1.93	0.24	...	3.00
NGC2403	10.94	0.83	0.00	10.73	0.86	...	14.14	0.51	...	1.00
NGC2683	1.89	0.60	0.70	1.01	0.88	0.44	3.37	0.55	0.73	2.00
NGC2841	1.58	0.60	0.66	1.36	0.91	1.10	1.52	0.81	0.93	1.00
NGC2903	6.67	0.43	0.00	7.45	0.62	...	20.64	0.21	...	1.00
NGC2915	0.71	0.41	0.00	0.63	0.56	...	4.02	0.32	...	2.00
NGC2955	4.21	0.36	0.91	4.45	0.40	0.88	3.91	0.37	0.84	1.00
NGC2976	0.33	0.48	0.00	0.46	0.91	...	1.73	0.35	...	2.00
NGC2998	1.47	0.36	0.00	3.74	0.87	...	2.94	0.82	...	1.00
NGC3109	0.23	0.50	0.00	0.28	2.05	...	4.13	0.21	...	1.00
NGC3198	1.31	0.52	0.00	1.72	0.88	...	2.06	0.77	...	1.00
NGC3521	0.20	0.52	0.00	0.77	0.71	...	0.51	0.46	...	1.00
NGC3726	2.54	0.61	0.00	2.41	0.76	...	2.98	0.47	...	2.00
NGC3741	0.90	0.71	0.00	0.65	0.71	...	0.77	0.31	...	1.00
NGC3769	0.88	0.43	0.00	0.71	0.71	...	0.95	0.41	...	2.00
NGC3877	3.47	0.31	0.00	9.07	0.87	...	10.22	0.40	...	2.00
NGC3893	0.69	0.46	0.00	0.57	0.73	...	1.00	0.45	...	1.00
NGC3917	1.64	0.53	0.00	2.70	1.14	...	4.60	0.55	...	1.00
NGC3949	0.84	0.52	0.00	0.76	0.73	...	0.55	0.44	...	2.00
NGC3953	0.56	0.49	0.00	0.76	0.90	...	3.42	0.59	...	1.00
NGC3972	0.80	0.45	0.00	2.08	1.03	...	2.07	0.50	...	1.00
NGC3992	0.71	0.55	0.00	1.68	1.04	...	3.47	0.76	...	1.00
NGC4010	2.16	0.46	0.00	1.90	0.85	...	2.74	0.36	...	2.00
NGC4013	0.84	0.58	0.83	1.53	0.54	1.43	1.81	0.35	0.79	2.00
NGC4051	1.73	0.48	0.00	1.91	0.81	...	2.49	0.45	...	2.00
NGC4068	0.82	0.49	0.00	0.27	0.80	...	2.52	0.38	...	2.00
NGC4085	5.28	0.36	0.00	2.83	0.58	...	9.09	0.35	...	2.00
NGC4088	0.64	0.46	0.00	0.87	0.63	...	0.66	0.40	...	1.00
NGC4100	1.21	0.57	0.00	1.90	0.95	...	1.66	0.76	...	1.00
NGC4138	5.52	0.55	0.68	0.75	0.98	0.00	2.49	0.55	0.69	2.00
NGC4157	0.45	0.53	0.66	0.61	0.69	0.56	0.72	0.43	0.64	1.00
NGC4183	0.14	0.53	0.00	0.53	1.24	...	1.13	0.79	...	1.00
NGC4214	0.77	0.50	0.00	1.19	1.01	...	1.06	0.46	...	2.00
NGC4217	2.23	0.60	0.30	1.33	1.13	0.46	3.17	1.17	0.17	1.00
NGC4389	6.30	0.29	0.00	0.20	0.31	...	9.31	0.30	...	3.00
NGC4559	0.35	0.50	0.00	0.34	0.77	...	0.50	0.52	...	1.00
NGC5005	0.10	0.49	0.60	0.07	0.62	0.69	0.09	0.54	0.56	1.00
NGC5033	7.15	0.52	0.36	6.39	0.85	0.52	8.02	1.03	0.43	1.00
NGC5055	6.19	0.26	0.00	6.29	0.62	...	7.42	0.56	...	1.00
NGC5371	1.96	0.42	0.00	12.55	0.78	...	10.16	3.30	...	1.00
NGC5585	5.18	0.55	0.00	6.35	0.75	...	6.82	0.22	...	1.00
NGC5907	3.30	0.42	0.00	7.88	0.94	...	7.73	1.08	...	1.00
NGC5985	2.54	0.53	0.64	5.91	1.01	2.12	6.97	0.63	3.32	1.00
NGC6015	9.28	0.64	0.00	13.06	0.99	...	10.87	1.12	...	2.00
NGC6195	1.81	0.41	0.79	2.95	0.41	0.81	2.26	0.32	0.85	1.00

Continued on next page

Table 11 – continued from previous page

MW: SXJ	DM	DM	DM	RCFM	RCFM	RCFM	RAR	RAR	RAR	
Galaxy	$\chi_r^2$	$\gamma_{disk}$	$\gamma_{bulge}$	$\chi_r^2$	$\gamma_{disk}$	$\gamma_{bulge}$	$\chi_r^2$	$\gamma_{disk}$	$\gamma_{bulge}$	Q
NGC6503	1.29	0.34	0.00	1.44	0.75	...	2.98	0.45	...	1.00
NGC6674	1.47	0.87	0.74	3.98	0.70	1.87	10.64	0.95	1.30	1.00
NGC6789	NAN	0.50	0.00	0.57	1.41	...	5.90	0.60	...	2.00
NGC6946	1.55	0.57	0.61	1.75	0.64	0.58	1.53	0.64	0.71	1.00
NGC7331	0.95	0.45	0.65	1.05	0.53	1.17	1.29	0.32	0.60	1.00
NGC7793	0.79	0.58	0.00	0.75	0.89	...	1.01	0.55	...	1.00
NGC7814	0.46	0.52	0.60	0.63	0.38	0.68	1.33	1.17	0.52	1.00
PGC51017	5.98	0.41	0.00	2.31	0.80	...	4.57	0.44	...	3.00
UGC00128	3.56	0.57	0.00	6.16	1.64	...	6.25	2.49	...	1.00
UGC00191	1.97	0.49	0.00	2.45	1.38	...	3.84	1.10	...	1.00
UGC00634	NAN	0.50	0.00	5.83	1.57	...	2.43	0.49	...	2.00
UGC00731	0.22	0.50	0.00	0.08	3.79	...	6.42	2.39	...	1.00
UGC00891	NAN	0.50	0.00	1.45	1.34	...	25.16	0.32	...	2.00
UGC01230	1.18	0.52	0.00	0.80	1.71	...	2.95	0.72	...	1.00
UGC01281	0.14	0.50	0.00	0.34	1.42	...	0.24	0.39	...	1.00
UGC02023	NAN	0.49	0.00	0.06	0.72	...	1.15	0.49	...	2.00
UGC02259	0.96	0.50	0.00	4.66	1.81	...	7.22	1.14	...	2.00
UGC02455	1.07	0.45	0.00	0.90	0.28	...	6.55	0.33	...	3.00
UGC02487	4.86	0.82	0.54	4.18	1.24	0.77	4.48	1.83	0.91	1.00
UGC02885	0.84	0.47	1.00	2.14	0.50	0.98	0.86	0.45	0.97	1.00
UGC02916	11.58	1.06	0.50	11.36	1.41	0.71	11.65	1.57	0.73	2.00
UGC02953	4.97	0.50	0.60	5.69	0.74	0.78	5.66	0.61	0.62	2.00
UGC03205	3.82	0.67	0.88	2.99	0.68	1.07	4.20	0.73	1.32	1.00
UGC03546	0.99	0.61	0.53	1.14	0.61	0.60	0.91	0.68	0.51	1.00
UGC03580	2.40	0.94	0.32	2.20	0.48	0.41	2.29	0.29	0.11	2.00
UGC04278	0.58	0.66	0.00	0.92	1.00	...	2.60	0.53	...	1.00
UGC04305	1.45	0.54	0.00	NAN	...	...	2.02	0.71	...	3.00
UGC04325	2.89	0.52	0.00	3.72	1.87	...	9.43	0.94	...	1.00
UGC04483	0.54	0.50	0.00	0.52	1.28	...	0.87	0.43	...	2.00
UGC04499	0.46	0.46	0.00	1.54	1.14	...	1.78	0.51	...	1.00
UGC05005	0.05	0.50	0.00	0.09	1.03	...	0.32	0.45	...	1.00
UGC05253	3.79	0.55	0.72	5.65	0.53	0.72	4.75	0.63	0.69	2.00
UGC05414	0.37	0.52	0.00	0.19	1.06	...	1.30	0.41	...	1.00
UGC05716	3.07	0.50	0.00	3.81	1.52	...	5.66	1.41	...	2.00
UGC05721	0.94	0.50	0.00	0.84	1.11	...	1.82	0.62	...	1.00
UGC05750	0.26	0.49	0.00	0.47	1.57	...	1.35	0.48	...	1.00
UGC05764	7.05	0.49	0.00	9.45	3.70	...	16.18	3.83	...	2.00
UGC05829	0.19	0.51	0.00	0.07	1.85	...	0.45	0.60	...	2.00
UGC05918	0.03	0.50	0.00	0.21	2.31	...	0.94	0.54	...	2.00
UGC05986	1.72	0.56	0.00	1.69	1.15	...	4.00	0.31	...	2.00
UGC05999	NAN	0.50	0.00	3.56	1.27	...	5.69	0.48	...	2.00
UGC06399	0.15	0.51	0.00	0.22	1.43	...	0.52	0.53	...	1.00
UGC06446	0.22	0.50	0.00	0.17	1.69	...	1.00	1.04	...	1.00
UGC06614	0.18	0.50	0.71	1.20	0.72	0.59	1.16	0.51	0.50	1.00
UGC06628	0.31	0.50	0.00	NAN	...	...	0.85	0.52	...	2.00

Continued on next page

Table 11 – continued from previous page

MW: SXJ	DM	DM	DM	RCFM	RCFM	RCFM	RAR	RAR	RAR	
Galaxy	$\chi_r^2$	$\gamma_{disk}$	$\gamma_{bulge}$	$\chi_r^2$	$\gamma_{disk}$	$\gamma_{bulge}$	$\chi_r^2$	$\gamma_{disk}$	$\gamma_{bulge}$	Q
UGC06667	0.39	0.51	0.00	2.41	3.77	...	5.36	1.00	...	1.00
UGC06786	0.69	0.35	0.78	0.69	0.50	0.66	1.39	0.27	0.34	1.00
UGC06787	18.09	0.90	0.19	24.78	0.73	0.57	20.81	0.45	0.28	2.00
UGC06818	2.10	0.45	0.00	1.24	0.53	...	5.39	0.29	...	2.00
UGC06917	0.39	0.48	0.00	1.09	1.12	...	1.32	0.54	...	1.00
UGC06923	1.97	0.48	0.00	0.88	0.80	...	1.62	0.42	...	2.00
UGC06930	0.22	0.52	0.00	0.55	1.25	...	1.23	0.63	...	1.00
UGC06973	1.45	0.31	0.60	0.41	0.36	0.81	15.58	0.17	0.39	3.00
UGC06983	0.58	0.51	0.00	0.77	1.26	...	1.39	0.77	...	1.00
UGC07089	0.23	0.51	0.00	0.15	0.95	...	0.43	0.36	...	2.00
UGC07125	0.40	0.50	0.00	1.18	1.08	...	1.60	0.92	...	1.00
UGC07151	1.58	0.56	0.00	1.30	1.15	...	3.75	0.50	...	1.00
UGC07232	NAN	0.50	0.00	0.76	0.82	...	6.17	0.46	...	2.00
UGC07261	0.16	0.47	0.00	1.46	1.22	...	0.83	0.56	...	2.00
UGC07323	0.43	0.51	0.00	0.26	0.97	...	0.66	0.41	...	1.00
UGC07399	0.36	0.50	0.00	1.00	1.54	...	1.90	0.59	...	1.00
UGC07524	0.34	0.53	0.00	1.48	1.59	...	1.84	0.79	...	1.00
UGC07559	0.26	0.50	0.00	0.21	0.97	...	2.60	0.31	...	2.00
UGC07577	0.22	0.49	0.00	0.06	0.67	...	5.79	0.24	...	2.00
UGC07603	0.47	0.48	0.00	0.52	1.07	...	1.77	0.34	...	1.00
UGC07608	0.14	0.50	0.00	0.30	2.02	...	0.73	0.48	...	1.00
UGC07690	0.87	0.53	0.00	0.40	1.05	...	1.53	0.60	...	2.00
UGC07866	0.12	0.50	0.00	0.07	1.26	...	0.26	0.45	...	2.00
UGC08286	1.00	0.52	0.00	2.66	1.66	...	2.64	1.05	...	1.00
UGC08490	0.21	0.51	0.00	0.15	1.26	...	0.34	0.86	...	1.00
UGC08550	0.55	0.50	0.00	0.70	1.35	...	1.55	0.74	...	1.00
UGC08699	0.87	0.75	0.59	0.95	0.55	0.76	0.99	0.63	0.70	2.00
UGC08837	0.68	0.49	0.00	0.69	0.78	...	2.35	0.20	...	2.00
UGC09037	1.09	0.30	0.00	1.55	0.58	...	2.26	0.20	...	2.00
UGC09133	6.78	0.65	0.53	7.50	0.77	0.72	6.94	1.64	1.10	1.00
UGC09992	NAN	0.51	0.00	0.04	1.30	...	1.08	0.51	...	2.00
UGC10310	0.64	0.51	0.00	0.12	1.54	...	1.76	0.62	...	1.00
UGC11455	2.40	0.41	0.00	3.98	0.76	...	6.55	0.38	...	1.00
UGC11557	0.67	0.48	0.00	0.91	0.60	...	3.18	0.42	...	2.00
UGC11820	3.46	1.19	0.00	1.44	1.24	...	1.99	1.01	...	1.00
UGC11914	0.65	0.42	0.75	1.61	0.07	0.89	1.73	0.22	0.48	1.00
UGC12506	0.29	0.59	0.00	1.18	1.35	...	1.98	1.12	...	2.00
UGC12632	0.17	0.50	0.00	0.21	1.86	...	1.80	1.08	...	1.00
UGC12732	0.24	0.48	0.00	0.18	1.51	...	0.50	1.07	...	1.00
UGCA281	0.38	0.49	0.00	0.28	1.23	...	0.47	0.37	...	3.00
UGCA442	1.60	0.50	0.00	0.86	2.28	...	7.65	0.44	...	1.00
UGCA444	0.22	0.50	0.00	0.10	3.78	...	0.33	0.49	...	2.00

## REFERENCES

- Battaglia, G., Fraternali, F., Oosterloo, T., , & Sancisi, R. 2006, *A&A*, 447, 49
- Bekenstein, J. D. 2004, *Phys. Rev. D*, 70, 083509, doi: [10.1103/PhysRevD.70.083509](https://doi.org/10.1103/PhysRevD.70.083509)
- Bell, E. F., & de Jong, R. S. 2001, *ApJ*, 550, 212, doi: [10.1086/319728](https://doi.org/10.1086/319728)
- Bosma, A. 1981, *AJ*, 86, 1791
- Boyer, T. H. 2011, *American Journal of Physics*, 79, 644, doi: [10.1119/1.3534842](https://doi.org/10.1119/1.3534842)
- Casertano, S. 1983, *MNRAS*, 203, 735, doi: [10.1093/mnras/203.3.735](https://doi.org/10.1093/mnras/203.3.735)
- Cebrián, S. 2022, in 10th Symposium on Large TPCs for Low-Energy Rare Event Detection. <https://arxiv.org/abs/2205.06833>
- Chatterjee, T. 1987, *Ap&SS*, 139, 243
- Cisneros, S., Goedecke, G., Beetle, C., & Engelhardt, M. 2015, *MNRAS*, 448, 2733, doi: [10.1093/mnras/stv172](https://doi.org/10.1093/mnras/stv172)
- Conroy, C., Gunn, J., & White, M. 2009, *ApJ*, 699, 486
- Cooperstock, F. I., & Tieu, S. 2007, *International Journal of Modern Physics A*, 22, 2293, doi: [10.1142/S0217751X0703666X](https://doi.org/10.1142/S0217751X0703666X)
- de Blok, W., & McGaugh, S. 1997, *MNRAS*, 290, 533
- de Blok, W., Walter, F., , & Brinks, E. 2008a, *AJ*, 136, 2648
- . 2008b, *AJ*, 136, 2648
- de Vaucouleurs, G. 1959, *Handbuch der Physik*, 53, 275, doi: [10.1007/978-3-642-45932-0\\_7](https://doi.org/10.1007/978-3-642-45932-0_7)
- Desmond, H., Bartlett, D. J., & Ferreira, P. G. 2023, *Monthly Notices of the Royal Astronomical Society*, 521, 1817, doi: [10.1093/mnras/stad597](https://doi.org/10.1093/mnras/stad597)
- Dutton, A. A., Courteau, S., de Jong, R., & Carignan, C. 2005, *The Astrophysical Journal*, 619, 218, doi: [10.1086/426375](https://doi.org/10.1086/426375)
- Dutton, A. A., Macciò, A. V., Obreja, A., & Buck, T. 2019, *Monthly Notices of the Royal Astronomical Society*, 485, 1886, doi: [10.1093/mnras/stz531](https://doi.org/10.1093/mnras/stz531)
- Famaey, B., & McGaugh, S. S. 2012, *Living Reviews in Relativity*, 15, 10, doi: [10.12942/lrr-2012-10](https://doi.org/10.12942/lrr-2012-10)
- Fich, M., & Tremaine, S. 1991, *ARA&A*, 29, 409, doi: [10.1146/annurev.aa.29.090191.002205](https://doi.org/10.1146/annurev.aa.29.090191.002205)
- Fraternali, F., Sancisi, R., , & Kamphuis, P. 2011, *A&A*, <http://arxiv.org/abs/1105.3867>
- Freeman, K. C. 1970, *ApJ*, 160, 811, doi: [10.1086/150474](https://doi.org/10.1086/150474)
- Gentile, G., Famaey, B., & de Blok, W. 2011, *A&A*, 527, A76
- Gentile, G., Józsa, G. I. G., Serra, P., et al. 2013, *A&A*, 554, A125, doi: [10.1051/0004-6361/201321116](https://doi.org/10.1051/0004-6361/201321116)
- Huré, J. M., & Hersant, F. 2011, *A&A*, 531, A36, doi: [10.1051/0004-6361/201015854](https://doi.org/10.1051/0004-6361/201015854)
- Jackson, J. 1999, *Classical Electrodynamics*, 3rd edn. (John Wiley & Sons, Inc., New Jersey, USA)
- Jetzer, P. 2017, *Physik-Institut der Universität Zurich*. [https://www.physik.uzh.ch/groups/jetzer/notes/PHY529\\_ART\\_III.pdf](https://www.physik.uzh.ch/groups/jetzer/notes/PHY529_ART_III.pdf)
- Jiao, Yongjun, Hammer, François, Wang, Haifeng, et al. 2023, *A&A*, 678, A208, doi: [10.1051/0004-6361/202347513](https://doi.org/10.1051/0004-6361/202347513)
- Keller, B. W., & Wadsley, J. W. 2017, *The Astrophysical Journal Letters*, 835, L17, doi: [10.3847/2041-8213/835/1/117](https://doi.org/10.3847/2041-8213/835/1/117)
- Lelli, F., McGaugh, S. S., & Schombert, J. M. 2016, *AJ*, 152, 157, doi: [10.3847/0004-6256/152/6/157](https://doi.org/10.3847/0004-6256/152/6/157)
- Lelli, F., McGaugh, S. S., Schombert, J. M., & Pawłowski, M. S. 2017, *The Astrophysical Journal*, 836, 152, doi: [10.3847/1538-4357/836/2/152](https://doi.org/10.3847/1538-4357/836/2/152)
- Li, P., Lelli, F., McGaugh, S., & Schombert, J. 2018, *Astronomy I& Astrophysics*, 615, A3, doi: [10.1051/0004-6361/201732547](https://doi.org/10.1051/0004-6361/201732547)
- Maschberger, T., Bonnell, I. A., Clarke, C. J., & Moraux, E. 2014, *Monthly Notices of the Royal Astronomical Society*, 439, 234, doi: [10.1093/mnras/stt2403](https://doi.org/10.1093/mnras/stt2403)
- McGaugh, S. 1999, *Conference Proceedings*, 182. [https://ned.ipac.caltech.edu/level5/McGaugh/Mcgaugh\\_contents.html](https://ned.ipac.caltech.edu/level5/McGaugh/Mcgaugh_contents.html)
- . 2014, *Galaxies*, 2, 601–622, doi: [10.3390/galaxies2040601](https://doi.org/10.3390/galaxies2040601)
- McGaugh, S. S. 2004, *ApJ*, 609, 652, doi: [10.1086/421338](https://doi.org/10.1086/421338)
- McGaugh, S. S. 2008, *The Astrophysical Journal*, 683, 137, doi: [10.1086/589148](https://doi.org/10.1086/589148)
- . 2021, *Studies in History and Philosophy of Science*, 88, 220, doi: <https://doi.org/10.1016/j.shpsa.2021.05.008>
- McGaugh, S. S., Lelli, F., & Schombert, J. M. 2016, *Phys. Rev. Lett.*, 117, 201101, doi: [10.1103/PhysRevLett.117.201101](https://doi.org/10.1103/PhysRevLett.117.201101)
- Milgrom, M. 1983, *ApJ*, 270, 371, doi: [10.1086/161131](https://doi.org/10.1086/161131)
- Misner, C. W., Thorne, K. S., & Wheeler, J. A. 1973, *Gravitation*
- Mistele, T., McGaugh, S., & Hossenfelder, S. 2022, *A&A*, 664, A40, doi: [10.1051/0004-6361/202243216](https://doi.org/10.1051/0004-6361/202243216)
- Naidu, R. P., Oesch, P. A., van Dokkum, P., et al. 2022, *The Astrophysical Journal Letters*, 940, L14, doi: [10.3847/2041-8213/ac9b22](https://doi.org/10.3847/2041-8213/ac9b22)
- Navarro, J. F., Benítez-Llambay, A., Fattahi, A., et al. 2017, *MNRAS*, 471, 1841, doi: [10.1093/mnras/stx170510.48550/arXiv.1612.06329](https://doi.org/10.1093/mnras/stx170510.48550/arXiv.1612.06329)
- Navarro, J. F., Frenk, C. S., & White, S. D. M. 1996, *ApJ*, 462, 563, doi: [10.1086/177173](https://doi.org/10.1086/177173)

- Oh, S.-H., De Blok, W., Walter, F., Brinks, E., & Kennicutt, R. C. 2008, *The Astronomical Journal*, 136, 2761
- Persic, M., Salucci, P., & Stel, F. 1996, *MNRAS*, 281, 27
- Pomarède, D., Tully, R. B., Graziani, R., et al. 2020, *Astrophys. J.*, 897, 133, doi: [10.3847/1538-4357/ab9952](https://doi.org/10.3847/1538-4357/ab9952)
- Rindler, W. 2013, *Essential Relativity: Special, General, and Cosmological* (Springer New York).  
<https://books.google.com/books?id=WTfnBwAAQBAJ>
- Rubin, V., Ford, W., & Thonnard, N. 1980, *ApJ*, 238, 471
- Rubin, V. C., Thonnard, N., & Ford, Jr., W. K. 1978, *ApJ*, 225, L107, doi: [10.1086/182804](https://doi.org/10.1086/182804)
- Salucci, P., Lapi, A., Tonini, C., et al. 2007, *Monthly Notices of the Royal Astronomical Society*, 378, 41, doi: [10.1111/j.1365-2966.2007.11696.x](https://doi.org/10.1111/j.1365-2966.2007.11696.x)
- Sanders, R. H. 2010, *The Dark Matter Problem: A Historical Perspective*
- Schombert, J., McGaugh, S., & Lelli, F. 2018, *Monthly Notices of the Royal Astronomical Society*, 483, 1496, doi: [10.1093/mnras/sty3223](https://doi.org/10.1093/mnras/sty3223)
- Schwarzschild, M. 1954, *AJ*, 59, 273, doi: [10.1086/107013](https://doi.org/10.1086/107013)
- Sofue, Y. 2013, *Mass Distribution and Rotation Curve in the Galaxy* (Oswalt, T. D. and Gilmore, G.), 985, doi: [10.1007/978-94-007-5612-019](https://doi.org/10.1007/978-94-007-5612-019)
- Tecchiolli, M. 2019, *Universe*, 5, doi: [10.3390/universe5100206](https://doi.org/10.3390/universe5100206)
- Tully, R. B., Courtois, H., Hoffman, Y., & Pomarède, D. 2014, *Nature*, 513, 71, doi: [10.1038/nature13674](https://doi.org/10.1038/nature13674)
- van Albada, T. S., Bahcall, J. N., Begeman, K., & Sancisi, R. 1985, *ApJ*, 295, 305, doi: [10.1086/163375](https://doi.org/10.1086/163375)
- Wald, R. 1984, *General Relativity* (University of Chicago Press, Chicago, IL, USA)
- Xue, X., et al. 2008, *AJ*, 684, 1143, doi: [10.1086/589500](https://doi.org/10.1086/589500)
- Zel'dovich, Y. B. 1968, *Soviet Physics Uspekhi*, 11, 381, doi: [10.1070/PU1968v011n03ABEH003927](https://doi.org/10.1070/PU1968v011n03ABEH003927)
- Željko Ivezić, Kahn, S. M., Tyson, J. A., et al. 2019, *The Astrophysical Journal*, 873, 111, doi: [10.3847/1538-4357/ab042c](https://doi.org/10.3847/1538-4357/ab042c)